AGU PUBLICATIONS

Geophysical Research Letters

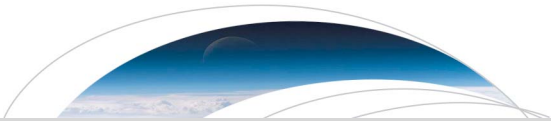

RESEARCH LETTER
10.1002/2017GL073802

Key Points:
- Uncertainty in simulated ozone is dominated by a few key reactions in both biomass burning and anthropogenic pollution plumes
- Uncertainty in PAN decomposition is key to controlling model ensemble spread in ozone change in biomass burning air masses
- Increased uncertainty at low temperatures results in a large increase in ensemble ozone spread, particularly from the NO + O_3 reaction

Supporting Information:
- Supporting Information S1

Correspondence to:
S. R. Arnold,
s.arnold@leeds.ac.uk

Citation:
Ridley, D. A., M. Cain, J. Methven, and S. R. Arnold (2017), Sensitivity of tropospheric ozone to chemical kinetic uncertainties in air masses influenced by anthropogenic and biomass burning emissions, *Geophys. Res. Lett.*, *44*, 7472–7481, doi:10.1002/2017GL073802.

Received 12 APR 2017
Accepted 30 MAY 2017
Accepted article online 2 JUN 2017
Published online 18 JUL 2017
Corrected 8 AUG 2017

This article was corrected on 8 AUG 2017. See the end of the full text for details.

Sensitivity of tropospheric ozone to chemical kinetic uncertainties in air masses influenced by anthropogenic and biomass burning emissions

D. A. Ridley[1,2], M. Cain[3], J. Methven[4], and S. R. Arnold[1]

[1]Institute for Climate and Atmospheric Science, School of Earth and Environment, University of Leeds, Leeds, UK, [2]Now at Department of Civil and Environmental Engineering, Massachusetts Institute of Technology, Cambridge, Massachusetts, USA, [3]Centre for Atmospheric Science, Department of Chemistry, University of Cambridge, Cambridge, UK, [4]Department of Meteorology, University of Reading, Reading, UK

Abstract We use a Lagrangian chemical transport model with a Monte Carlo approach to determine impacts of kinetic rate uncertainties on simulated concentrations of ozone, NO_y and OH in a high-altitude biomass burning plume and a low-level industrial pollution plume undergoing long-range transport. Uncertainties in kinetic rate constants yield 10–12 ppbv (5th to 95th percentile) uncertainty in the ozone concentration, dominated by reactions that cycle NO and NO_2, control NO_x conversion to NO_y reservoir species, and key reactions contributing to O_3 loss ($O(^1D) + H_2O$, $HO_2 + O_3$). Our results imply that better understanding of the peroxyacetylnitrate (PAN) thermal decomposition constant is key to predicting large-scale O_3 production from fire emissions and uncertainty in the reaction of NO + O_3 at low temperatures is particularly important for both the anthropogenic and biomass burning plumes. The highlighted reactions serve as a useful template for targeting new laboratory experiments aimed at reducing uncertainties in our understanding of tropospheric O_3 photochemistry.

Plain Language Summary Computer models used to assess and predict how air pollution changes in response to emissions, and how it affects climate and human health, rely on information from laboratory experiments to prescribe the rates at which different atmospheric chemical species react. This laboratory information has uncertainties associated with experimental limitations or constraints. We show how these uncertainties affect confidence in model predictions of tropospheric ozone in two pollution plumes. Ozone is a key air pollutant, harmful to human health and vegetation, as well as a climate warming agent. We identify key reactions that lead to large uncertainty in simulated ozone and demonstrate the importance of low confidence in some reactions at low temperatures in driving large portion of ozone uncertainty. Our work serves as a key basis from which to motivate future lab experiments aimed at reducing uncertainty in our understanding of tropospheric ozone.

1. Introduction

Atmospheric chemistry processes control the distribution and abundance of trace constituents that affect both climate and air quality. Tropospheric ozone (O_3) is a greenhouse gas and air pollutant, harmful to human health [e.g., *Levy et al.*, 2001; *Ito et al.*, 2005] and detrimental to vegetation and crops [*Sitch et al.*, 2007; *Van Dingenen et al.*, 2009; *Hollaway et al.*, 2012]. Ozone is produced in situ in the troposphere by photochemical oxidation of volatile organic compounds (VOCs) in the presence of nitrogen oxides (NO_x = NO + NO_2). Globally, photolysis of O_3 is the chief source of the OH radical [*Logan et al.*, 1981; *Lelieveld et al.*, 2002], controlling the lifetime of the greenhouse gas methane [*Myhre et al.*, 2013], and oxidation of gas-phase aerosol precursors [*Kroll and Seinfeld*, 2008]. Once exported to the free troposphere where it has a lifetime of several weeks, O_3 can undergo long-range transport between continents [*Jacob et al.*, 1999; *Jaffe et al.*, 2003; *Stohl et al.*, 2003; *Price et al.*, 2004]. A robust understanding of O_3 photochemistry during continental export is central to our ability to predict response of the large-scale distribution of tropospheric ozone and OH to changes in continental emissions of NO_x and VOCs, and to our estimates of contributions from long-range transport of O_3 and precursors to surface O_3 in a given region. Aggressive emissions reductions in Europe and the U.S. have resulted in a decrease in the frequency of peak O_3 levels since the 1990s [*Lin et al.*, 2001; *Soldberg and Lindskog*, 2005]. However, overall emissions of O_3 precursors in the Northern

Hemisphere (NH) are expected to continue to rise as economies in South and East Asia grow rapidly [*Zhang et al.*, 2009]. This is likely to lead to an increasing relative sensitivity of air quality in the western U.S. and Europe to O_3 formed upstream and imported during long-range transport events [*Parrish et al.*, 2009; *Verstraeten et al.*, 2015].

Models of atmospheric chemistry underpin our predictions of responses of climate and air quality to changes in anthropogenic and natural emissions. Model photochemical processes rely on data from laboratory experiments to parameterize the kinetics of chemical reactions, which are generally recommended by expert panels, based on the latest and best available laboratory data from the literature (the NASA Jet Propulsion Laboratory (JPL) [*Burkholder et al.*, 2015] and the International Union of Pure and Applied Chemistry (IUPAC) [*Atkinson et al.*, 2004; *Crowley et al.*, 2010] recommendations). The data from lab experiments used in such recommendations have uncertainties associated with experimental constraints and specific aspects of a given reaction system. Routinely, information regarding uncertainties in these parameters is not considered in model predictions; however, their impacts could potentially lead to uncertainties in simulation of key species concentrations important for climate and air quality. Here we focus specifically on the impact of kinetic data uncertainties in reactions of gas-phase HO_y, NO_y, and organic species on O_3 photochemistry in polluted plumes undergoing long-range transport. We use a Lagrangian chemical transport model and Monte Carlo ensemble approach to simulate photochemistry in two contrasting anthropogenic and biomass burning plumes. We quantify sensitivity of simulated concentrations of O_3 and key precursors to model kinetic parameter uncertainties using aircraft observations to provide model initialization and an observational comparison with model ensemble spread. We partition simulated uncertainty between specific reaction rates and identify key kinetic parameters that dominate the uncertainty in simulated oxidant photochemistry in the plumes and compare this uncertainty with that due to physical processes.

2. Methodology

2.1. Plume Cases and Modeling Framework

We examine two plume case studies, based on air masses sampled sequentially on multiple occasions by aircraft during the ICARTT (International Consortium for Atmospheric Research on Transport and Transformation) campaign in summer 2004 [*Fehsenfeld et al.*, 2006]. This pseudo-Lagrangian observation framework allows monitoring of air mass chemical evolution over several days [*Methven et al.*, 2006]. We use the CiTTyCAT Lagrangian chemistry model [*Evans et al.*, 2000; *Pugh et al.*, 2012; *Arnold et al.*, 2015], which includes inorganic NO_x, O_x, and HO_x chemistry, along with a treatment of methane and NMHC oxidation and comprises 90 species and 220 reactions (see supporting information for more details) to simulate tropospheric chemistry between aircraft observation points, and the sensitivity of this chemistry to kinetic parameter uncertainties. Air mass trajectories for the ICARTT Lagrangian Cases 2 and 3 [*Methven et al.*, 2006] are calculated using the ROTRAJ (Reading Offline Trajectory) Lagrangian transport model [*Methven et al.*, 2003] and initialized with species concentrations observed within the matching time windows of *Cain et al.* [2012]. We label Lagrangian Case 2 as "biomass burning upper troposphere (BBU)" and Case 3 as "anthropogenic pollution low level (APL)". A similar Lagrangian model framework was found to capture observed changes in O_3 and precursors in the same BBU case [*Real et al.*, 2007] and APL case [*Real et al.*, 2008]. *Cain et al.* [2012] used a CiTTyCAT model ensemble trajectory framework to examine the sensitivity of photochemical evolution to the representation of physical processes in these cases. Here the focus is on quantifying parametric model uncertainty associated with photochemical rates.

2.2. Perturbed Ensemble Methodology

The CiTTyCAT model framework has been modified to allow Monte Carlo ensemble simulations of each plume case, where each ensemble member considers a unique systematic perturbation of kinetic rate parameters in the model, per temperature-dependent parameter uncertainty estimates from the literature. Model rate constants and their uncertainties are taken from the JPL [*Burkholder et al.*, 2015] and IUPAC [*Atkinson et al.*, 2004; *Crowley et al.*, 2010] gas kinetic data recommendations and are used to set up a probability space that can be sampled by running the model with combinations of perturbed rate constants. The Latin hypercube (LHC) method [*Mckay et al.*, 2000] is used to efficiently sample the parameter space and to define ensemble perturbations. Since computational limitations prevent simulation of combinations of perturbations across the whole parameter space of 261 reaction rate constants, we first perform a set of

simulations probing the one-at-a-time effect of each reaction rate constant uncertainty on O_3 and OH evolution in the plumes. From these we identify a smaller set of 73 rate constant uncertainties that have largest impacts on O_3 and OH, for a full Monte Carlo simulation framework, allowing us to account for interdependencies between uncertainties in the reaction rate constants. A 2500-member ensemble was found to be sufficient to produce robust estimates of plume concentration uncertainty (see supporting information for details).

For a given reaction, the reaction rate constant, k, is commonly given by

$$k(T) = k_0 e^{-\frac{\Delta E}{RT}} \tag{1}$$

where k_0 is the prefactor, ΔE is the activation energy, T is the temperature, and R is the universal gas constant. The uncertainties in reaction rate constants are documented in the IUPAC and JPL recommendations, along with their temperature dependence. We use IUPAC recommendations for those rate constants that are not available in the JPL documentation.

The uncertainty of the rate constant increases as the temperature diverges from 298 K. The uncertainty on a given rate constant, *f(T)*, is calculated using the formula provided by JPL data sheets:

$$f(T) = f(298\ K)\exp^{\left|g\left(\frac{1}{T}-\frac{1}{298}\right)\right|} \tag{2}$$

where *f(*298 K*)* is the uncertainty factor at 298 K and g is an uncertainty parameter, both provided in the data sheets. The 1σ uncertainty at a temperature, T, is obtained by multiplying the rate, *k(T)*, by the uncertainty factor, *f(T)*. If the reaction rate is unavailable in the JPL data sheets, we use IUPAC and the following reaction rate uncertainty formula from *Atkinson et al.* [2004]:

$$\Delta \log k(T) = \Delta \log k(298\ K) + 0.4343\left\{\frac{\Delta E}{R}\left(\frac{1}{T}-\frac{1}{298}\right)\right\} \tag{3}$$

where $\Delta \log k(T)$ is the 2σ uncertainty of the reaction rate constant at temperature, T. In both cases, the uncertainty as a function of temperature is not determined by rigorous statistical analysis, but through subjective assessment by evaluators.

The model ensembles are run both with and without temperature dependence of the rate constant uncertainties included in equations (2) and (3). Comparing these two sets of ensembles gives information on the uncertainty in plume chemistry introduced by the poorer knowledge of kinetic parameters at temperatures farther from 298 K. For further details of the ensemble simulation method see supporting information.

We determine the reaction rates that produce the majority of the uncertainty in simulated O_3 using a multiple linear regression for each of the reaction rates as a function of the simulated perturbation to the O_3 concentration. As meteorological and chemical conditions change over the duration of plume transport, the effect of rate constant uncertainties is assessed after 2, 3, and 6 days of trajectory transport to evaluate the time dependence of the uncertainty in simulated O_3.

3. Results

3.1. Evolution of Ozone Uncertainty

Figures 1 and 2 show the time evolution of O_3, NO_y, CO, and OH in the simulated APL (anthropogenic pollution low-level) and BBU (biomass burning upper troposphere) air masses, respectively. The plotted envelopes display the 5th, 25th, 75th, and 95th percentile concentrations based on 2500 model simulations. The range of aircraft observations from downstream interception of the air masses are shown as vertical bars, representing one standard deviation on either side of the mean observed concentrations in each Lagrangian match window [*Cain et al.*, 2012].

The spread of O_3 concentrations produced by the kinetic uncertainties in the APL case (Figure 1a) increases rapidly after around 0.7 days, at the onset of daylight. Peroxyacetylnitrate (PAN) shows the largest fractional spread of the NO_y species, partly reflecting the spread in its precursor NO_2, as well as uncertainties in the specific rate of its formation (see section 3.3.1). Large spread in the nighttime NO_y reservoir species N_2O_5 partly results from ensemble spread in its precursor species (including production of NO_3, which is impacted by ensemble spread in both NO_2 and O_3). Spread in N_2O_5 appears to be a key driver of spread in daytime NO_x, due to the reformation of NO_2 from N_2O_5 at sunrise. This reformation of NO_2 is limited by heterogeneous

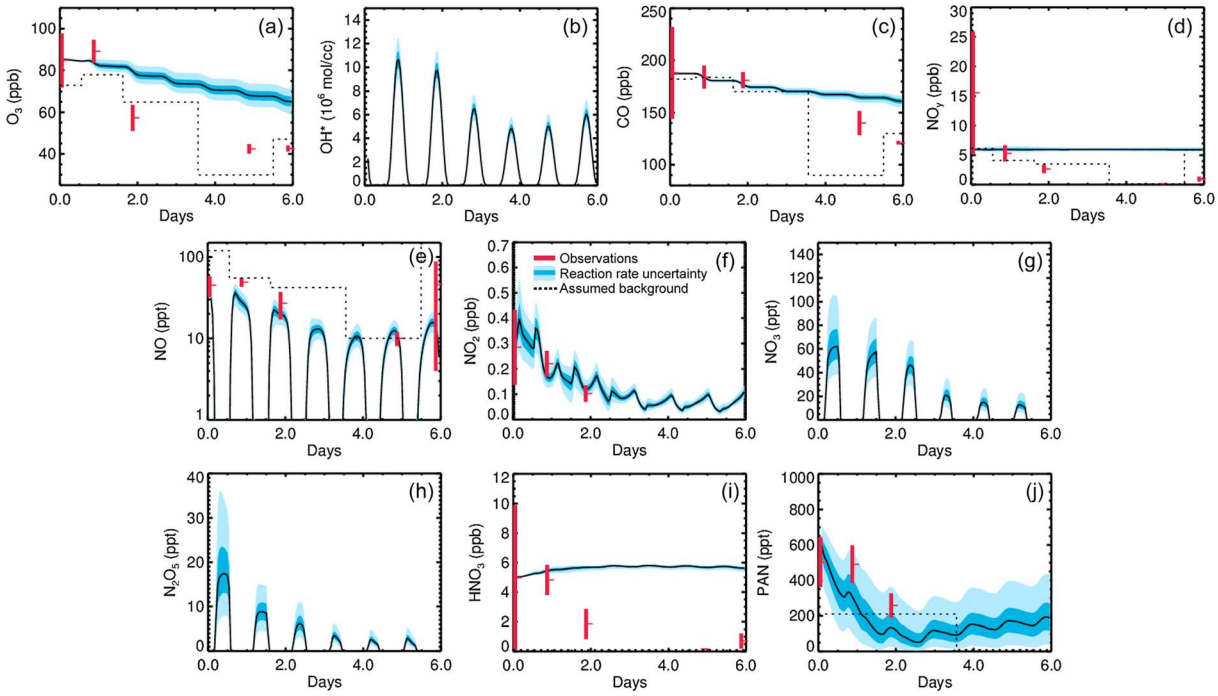

Figure 1. Time evolution of simulated ozone, OH, CO, and NO_y concentrations in the APL air mass, with uncertainty ranges based on 10 Monte Carlo model ensembles, each comprising 500 perturbed rate simulations. Median ensemble concentrations are shown in black. Dark blue and light blue shading show 25th to 75th percentile and 5th to 95th percentile ranges, respectively. Red vertical bars and symbol show observed standard deviation and mean concentrations observed by ICARTT campaign aircraft within the air mass [*Real et al.*, 2007, 2008]. Black dashed lines indicate the background concentration assumed in the model, based on ICARTT observations [*Real et al.*, 2007, 2008]. Note that simulated air mass dilution with background air and surface deposition mean that total NO_y is not conserved.

conversion of N_2O_5 to nitric acid (HNO_3) overnight. O_3 spread increases to 5.6 ppbv (from the 5th to 95th percentile) by the end of the first 24 h and continues to increase throughout the simulation, reaching 9.6 ppbv after 3 days, and a maximum of 11.9 ppbv at the end of the 6 day simulation. NO_2 concentrations and their spread decrease after day 3, as concentrations of NO_2 reservoir species (PAN and N_2O_5) reduce substantially. Although ensemble spread in OH (Figure 2b) does contribute to spread in CO (Figure 2c), the effect is small (11.1 ppbv) due to the long CO lifetime (approximately 90 days in this air mass). CO loss is dominated by plume dilution with surrounding background air. We assume a piecewise constant background concentration based on the observations [*Real et al.*, 2008]. Impacts of mixing assumptions on simulated air mass chemistry are discussed in section 3.2.

Ensemble spread in O_3 is initially small in the BBU case (Figure 2a) and begins to expand after around 2.3 days to reach a maximum spread of 9.9 ppbv (from the 5th to 95th percentile) after 5.8 days. The increase in spread corresponds with the time when the air mass begins to descend in altitude, reaching warmer temperatures (see supporting information Figure S1), promoting the thermal decomposition of PAN to reform NO_2. This effect can be seen in Figures 2f and 2j, showing the time series of NO_2 and PAN. The spread in NO_2 and PAN increases onward from 2.3 days, reaching respective spreads of 0.14 ppbv after 3.0 days and 0.44 ppbv after 6.0 days. Ensemble spread in PAN decomposition rate is the key determinant of O_3 spread in this plume, due to PAN's role as the source of NO_2 for O_3 production (see section 3.3.2). From the same point in time, spread in HNO_3 increases, due to the increased ensemble spread in NO_2 and OH. Spread in OH again produces small spread in CO (7.2 ppbv) due to its long chemical lifetime. *Real et al.* [2007] showed that dilution with background air dominates loss in CO in this case, as also discussed for the APL case. As in the APL case, spread in N_2O_5 and NO_3 are also evident in the BBU case, contributed to by the spread in NO_2 and O_3. *Cain et al.* [2012] also showed increased sensitivity to physical parameters after the initial 2 days of simulation of the BBU case. Modeled mixing rates, in particular, impacted chemical O_3 production through dilution of O_3 precursor concentrations, producing O_3 concentrations that were 3 up to ppbv higher (lower) with weaker (stronger) mixing.

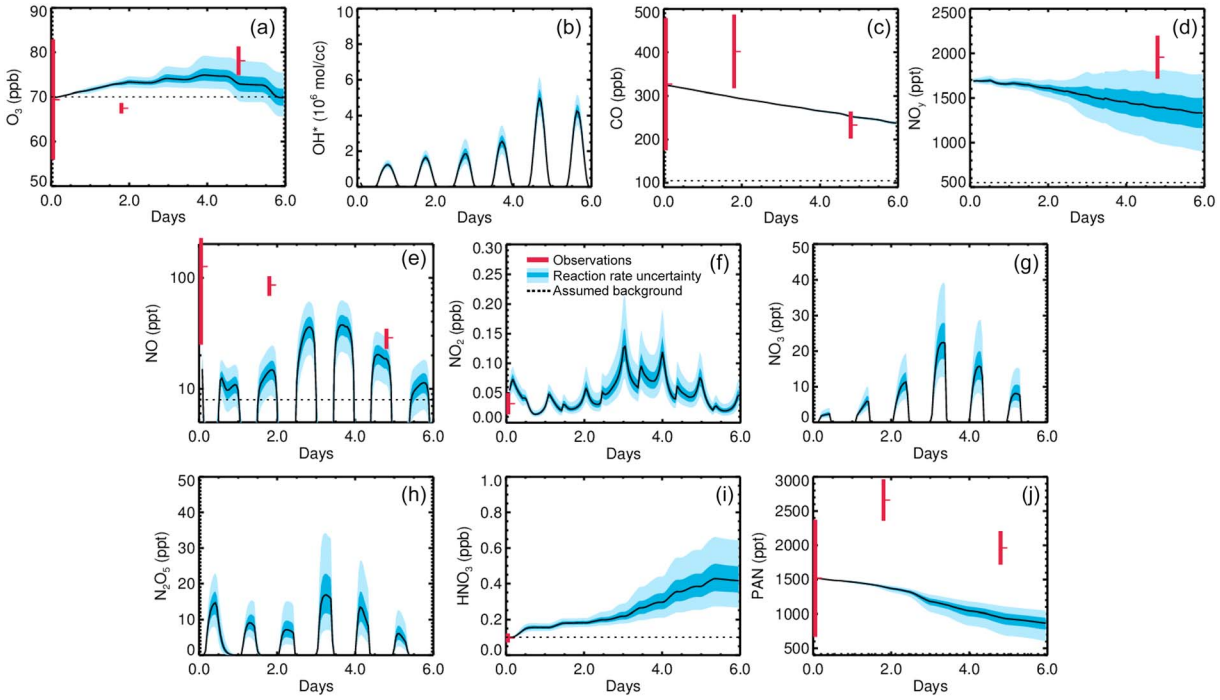

Figure 2. As in Figure 1 but for the BBU air mass simulations.

There is good agreement between the model and observations from the P3 and Falcon aircraft within Lagrangian match windows of NO, NO_2, PAN, and CO for the APL Case (Figure 1). However, the trajectory used has a high bias in water vapor of approximately 5 g/kg, and both O_3 and CO do not decline as rapidly as observed along the trajectory. The model does not reproduce the observed factor of 5 decline in HNO_3 concentration that the observations suggest, similar to *Real et al.* [2008]. This is likely explained by a lack of dry deposition in the model trajectory; *Cain et al.* [2012] show that transition of the air mass into the boundary layer can yield rapid dry deposition of HNO_3, with wet deposition playing a secondary role. For the BBU case, the model overestimates observed O_3 and NO, while underestimating CO and PAN. However, the model ensemble encompasses observed O_3, NO, and total NO_y after 4.5 days, while PAN remains underestimated (a consequence of the large uncertainty in PAN concentrations from which the model is initialized). Despite the underestimate in observed absolute PAN concentration, the upper range of simulated PAN lost to thermal decomposition (which provides a source of NO_2 to the air mass) during descent of the air mass is on the same order as that observed (ensemble range 270–790 pptv versus ~700 pptv observed between match windows). *Cain et al.* [2012] explored the sensitivity of CiTTyCAT model concentrations in these cases to uncertainties in initial conditions of the trajectory and found a model spread between 10 and 30 ppbv for O_3 in the APL case and an initial spread of 40 ppbv for the BBU case that tended toward a spread of 10 ppbv by the end of the simulation. The model sensitivity to different physical parameters and VOC chemistry produced up to a 5 ppbv and a 7 ppbv range of O_3 mixing ratios in the BBU case, respectively, and up to 20 ppbv for both sensitivities in the APL case. These uncertainties confound comparison with observations; however, the broad agreement with observed air mass chemical changes suggests that the key chemical processes are being captured sufficiently well to explore the sensitivity of the simulated O_3 to individual reaction rate kinetics.

3.2. Influence of Mixing

We explore the sensitivity of the simulated concentrations and spread of species resulting from kinetic uncertainties to the rate of mixing between the plume and background concentrations. For the standard APL simulation, we assume a polluted layer depth of 1500 m and use the 50th percentile mixing rate (κ_{mid} = 1.2 m^2 s^{-1}) derived from observed changes in VOC ratios within the air mass from

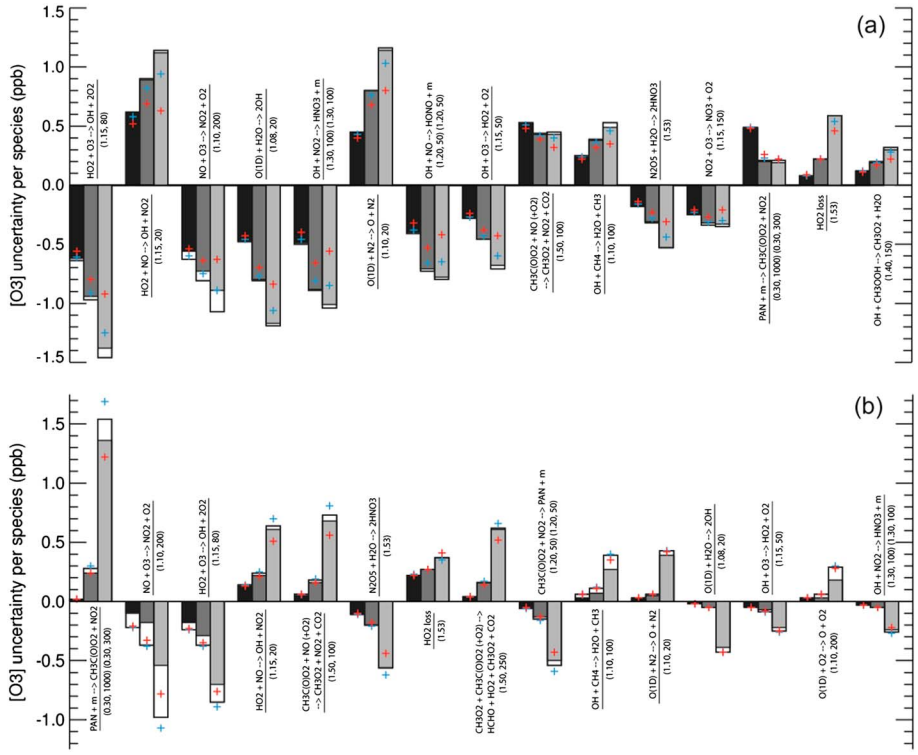

Figure 3. Air mass ozone uncertainty resulting from 1 sigma uncertainties in different reaction rates after 2 (black), 3 (dark grey) and 6 days (light grey), derived from Monte Carlo model ensembles comprising 2500 perturbed rate simulations for (a) the APL case and (b) the BBU case. Reactions are ordered by the average contribution to the O_3 uncertainty over the 6 day period. Solid bars show ozone response based on application of reaction rate uncertainties at 298 K. Unfilled parts of each bar show the uncertainty contribution resulting from temperature dependence of the rate parameter uncertainties. The uncertainty when using the 25th and 75th percentile mixing rates are shown as the blue and red crosses, respectively. The underlined reactions appear in both cases. The reaction rate uncertainty factors, *f*(298 K) and *g*, are included in brackets under the reaction for reference. There are two sets of uncertainty factors for the termolecular reactions and the 1 sigma uncertainty on the gamma factor is shown for the heterogenous reactions. See text for details.

Arnold et al. [2007] and we repeat the simulations with the 25th and 75th percentile values of the mixing rate (κ_{slow} = 0.52 m^2 s^{-1} and κ_{fast} = 1.56 m^2 s^{-1}). Both the slower and faster mixing rates cause the O_3 concentration to drop more rapidly, yielding 8% and 12% less ozone after 6 days (see Figures S2 and S3). The spread in the O_3 concentration owing to the reaction rate constant uncertainties is also reduced for both mixing rate limits (the spread in O_3 is 8.8 ppbv for the slower mixing rate and 7.6 ppbv for the higher mixing rate after 3 days). Faster mixing reduces O_3 directly through relaxation to lower background O_3 concentrations. In the slower mixing case, NO_2 is suppressed compared with the standard case, due to slower mixing of elevated background NO into the air parcel, as well as less mixing of PAN into the air mass at day ~3, resulting in slower photochemical O_3 formation. Reduction in ozone is therefore due to physical mixing of ozone in one case, and due to chemical response to lower NO_x (due to less mixing) in the other case. Since loss of O_3 is driven by first-order kinetics (i.e., it is dependent on the concentration of O_3 itself), the stronger decrease in O_3 over the course of the trajectory likely also limits the simulated spread in O_3. For the BBU case, mixing has less influence on the ensemble O_3 simulation. The 25th, 50th, and 75th percentile mixing rates from *Arnold et al.* [2007] are κ_{slow} = 0.65 m^2 s^{-1} κ_{mid} = 0.91 m^2 s^{-1}, and κ_{fast} = 1.56 m^2 s^{-1}, respectively. In this case the O_3 concentration is changed by <1% for each mixing scenario (see Figures S4 and S5). The spread in O_3 is increased by 6% after 3 days for the slower mixing rate and reduced by 11% for the faster mixing rate.

3.3. Rate-Specific Ozone Uncertainty

The perturbation in O_3 resulting from a 1σ change in each reaction rate can be estimated by linear regression of the O_3 concentration at a given time against the set of perturbed rates used. These O_3

sensitivities (Figure 3) are calculated at 2, 3, and 6 days into the plume transport to show the relative importance of each rate uncertainty as chemistry evolves. Reactions are ranked based upon the average contribution to the O_3 uncertainty over the 6 day simulation period. The results from the fixed-temperature ensembles are used to determine how much of the uncertainty can be attributed to temperature by taking the difference in the O_3 perturbation between ensembles using uncertainties with full reaction rate temperature dependence and those simply assuming uncertainties based on 298 K. The uncertainty in O_3 resulting from temperature effects is shown as the unfilled part of the bars in Figure 3. The effect of the temperature uncertainty is greater in the BBU case than in the APL case, since the ambient temperature stays closer to 298 K in the APL case (temperature, pressure, and water vapor for the simulation are displayed in Figure S1).

3.3.1. APL Case

For the APL case, uncertainty in O_3 is dominated by uncertainty in reactions controlling O_3 loss (reaction of $HO_2 + O_3$ and loss of $O(^1D)$ through reaction with H_2O), and fundamental reactions governing the cycling and loss of NO_x ($HO_2 + NO$; $NO + O_3$; $OH + NO_2$). These reactions are key in determining the net change in O_3 through their controls on O_3 loss and the NO_2 abundance. The impact of these rate uncertainties on O_3 increases by 20–40% between day 2 and day 3 and then by a similar percentage again by day 6. Uncertainty in the reaction of $HO_2 + NO$ produces comparable, but opposite sign response in O_3 to the $HO_2 + O_3$ loss reaction uncertainty. Six day O_3 responses to uncertainties in $O(^1D) + H_2O$, $NO + O_3$, and $OH + NO_2$ are of comparable magnitudes (1.04–1.19 ppbv), with temperature dependence of the $NO + O_3$ uncertainty increasing the O_3 uncertainty by 20%. Impact of the uncertainty in the quenching of $O(^1D)$ to $O(^3P)$ is comparable but opposite in sign to that in the $O(^1D) + H_2O$ reaction, due to the importance of the competition between these reactions in controlling net O_3 loss. Although we apply uncertainties in absolute rate constants for $O(^1D)$ reactions, since these are recommended in the JPL assessment, we note that there are smaller uncertainties quoted for relative $O(^1D)$ rate constants determined in some studies [e.g., *Carl*, 2005].

Uncertainties in reactions that play a role in the interconversion of PAN and its precursors are relatively more important on short timescales in the APL case. Uncertainty in PAN decomposition and in the reaction of $MeCO_3$ with NO both contribute a positive perturbation to O_3 of approximately 0.5 ppbv on a 2 day timescale; the latter being a route for cycling NO to NO_2, competing with NO_2 loss via $MeCO_3 + NO_2$. On longer timescales, these reactions become less important in this air mass as NO_2 concentrations decline and the warm, moist environment favors loss of NO_2 via reaction with OH to form HNO_3. Uncertainty in this reaction contributes an O_3 uncertainty of more than 1.0 ppbv after 6 days. Uncertainty in the reaction of $OH + CH_4$ produces the same but opposite sign O_3 response to the heterogeneous hydrolysis of N_2O_5 (+0.53 and −0.53 ppbv respectively after 6 days), due to their respective roles in supply of peroxy radicals and loss of NO_x.

The mixing rate assumed for the air mass has no significant impact on the relative importance of reaction rates for the APL case. However, the mixing sensitivity tests show a decrease in the O_3 uncertainty of up to 18% when the slower mixing rate is used and up to 47% decrease when the faster mixing rate is used.

3.3.2. BBU Case

Uncertainty in net O_3 change in the BBU case on a 6 day timescale is dominated by the uncertainty in the PAN decomposition rate, producing an O_3 sensitivity of more than 1.5 ppbv. This is the largest 1 sigma sensitivity overall in this simulated case. Increased O_3 response to this rate constant uncertainty later in the transport event occurs due to descent of the air mass to warmer temperatures, promoting decomposition of PAN to release NO_2. As in the APL case, uncertainty in the reactions of $NO + O_3$ and $MeCO_3 + NO$ also produces a large O_3 sensitivity after 6 days (0.98 and 0.73 ppbv magnitude, respectively), due to their roles in NO to NO_2 cycling, and the latter's competition with PAN formation. Reaction of $MeCO_3$ with CH_3O_2 directly competes with the PAN formation reaction, and uncertainty in this reaction produces a substantial O_3 response in the BBU case after 6 days (0.62 ppbv). Uncertainty in the $HO_2 + NO$ reaction, a key route for cycling of NO to NO_2, produces a response of similar magnitude after 6 days.

After only 2 days, PAN is stable due to lower temperatures in the upper troposphere, and uncertainty in the PAN decomposition rate produces a smaller O_3 uncertainty. Two day O_3 response is dominated by uncertainty in reactions determining ozone loss, particularly $NO + O_3$ and $HO_2 + O_3$.

The BBU case demonstrates substantial effects of increased kinetic uncertainties at lower temperatures (white bars in Figure 3b). This sensitivity is due to temperatures in the UT air mass being substantially lower than 298 K, at which kinetic parameter uncertainty is minimum [*Burkholder et al.*, 2015]. Sensitivity to the temperature dependence of the uncertainty in the rate of NO + O_3 is substantial, increasing the O_3 response to uncertainty in this reaction by between 45 and 55%, contributing an O_3 sensitivity after 6 days of 0.44 ppbv of a total of 0.98 ppbv. The documented temperature dependence of uncertainty in this reaction is slightly larger than other key reactions (e.g., 21% at 260 K, compared with 16% for the HO_2 + NO reaction) and increases with temperature deviation from 298 K at a faster rate [*Burkholder et al.*, 2015]. Temperature effects on O_3 uncertainty are also substantial for PAN decomposition and HO_2 + O_3 reactions after 6 days, increasing the O_3 uncertainty by 11% and 12%, respectively.

The mixing rate assumed for the air mass has no significant impact on the relative importance of reaction rates, as with the APL case. The effect of uncertainty in mixing is weaker in the BBU case, with slower mixing contributing up to a 10% increase in the O_3 uncertainty and faster mixing up to a 20% decrease.

4. Discussion and Conclusions

The range in simulated ozone concentrations due to kinetic uncertainties is 9.9 and 11.9 ppbv (5th to 95th percentile) for the BBU and APL cases, respectively. This is several times larger than estimates of the Asian contribution to surface O_3 concentrations over the North American West Coast (~1–4 ppbv) [*Brown-Steiner and Hess*, 2011; *Sudo and Akimoto*, 2007] from long-range transport, and an order of magnitude larger than estimates of the annual trend in O_3 in this region from increases in trans-Pacific inflow [*Verstraeten et al.*, 2015; *Cooper et al.*, 2010; *Parrish et al.*, 2009]. The range in ozone is comparable with intermodel standard deviation in present-day surface and lower tropospheric ozone concentrations among current generation global models of tropospheric chemistry [*Young et al.*, 2013].

Our results imply particularly poor constraint on our knowledge of ozone chemistry in biomass burning plumes transported to the upper troposphere. This may have important implications for simulating tropospheric oxidant chemistry in the tropical troposphere, where biomass burning emissions are rapidly transported vertically in deep convection and are an important source of ozone and precursors [*Anderson et al.*, 2016; *Singh et al.*, 2000; *Folkins et al.*, 1997]. Uncertainty in biomass burning emission impacts on upper tropospheric ozone has important implications for our confidence in radiative forcing from anthropogenic changes in tropospheric ozone [*Rap et al.*, 2015].

Uncertainty in simulated O_3 in the two air masses is dominated by kinetic uncertainties in reactions that cycle NO and NO_2, reactions controlling conversion of NO_x to NO_y reservoir species, plus key reactions contributing to O_3 loss ($O(^1D)$ + H_2O, HO_2 + O_3). Twelve of the fifteen leading rate constant uncertainties contribute to O_3 uncertainty in both the APL and BBU cases (underlined in Figure 3). The large PAN loading of the BBU case and air mass descent to warmer temperatures means that O_3 production in this plume is highly sensitive to uncertainty in the rate of PAN thermal decomposition. Large PAN loadings are commonly observed in biomass burning plumes, meaning that understanding of O_3 production from biomass burning emissions on a large scale may be sensitive to this rate uncertainty. Uncertainty in the rate of O_3 + NO is a key driver of O_3 uncertainty in both cases, and the larger uncertainty of this reaction rate at low temperatures produces considerable uncertainty, particularly in the upper tropospheric BBU case. The reaction of HO_2 + NO ranks highly in its contribution to plume O_3 uncertainty in both cases, illustrating its crucial role in determining available NO_2 for O_3 production.

Chemical transport models routinely use the same kinetic rate constants provided by the JPL and IUPAC assessments used here. The uncertainty in O_3 that we have demonstrated may therefore represent a so-far uncharacterized error or bias across model O_3 estimates. Improved confidence in the rate parameters for these fundamental reactions, and particularly their temperature dependence in the case of NO + O_3, would allow substantial reduction in O_3 production rate uncertainty. Overall, our results provide a framework for targeting new laboratory experiments aimed at reducing uncertainties in our understanding of tropospheric O_3 photochemistry.

Acknowledgments

This work was supported by the UK Natural Environment Research Council (award NE/F00060X/1) and also the UK contribution to the ICARTT experiment through the NERC ITOP project NER/T/S/2002/00580. The authors acknowledge all groups involved in the ICARTT campaigns. Please see http://www.esrl.noaa.gov/csd/ICARTT/participants/. Model ensemble data are available from University of Leeds on request. Aircraft observations are available via campaign references cited.

References

Anderson, D. C., et al. (2016), A pervasive role for biomass burning in tropical high ozone/low water structures, *Nat. Commun.*, *7*, 10,267, doi:10.1038/ncomms10267.

Arnold, S. R., et al. (2007), Statistical inference of OH concentrations and air mass dilution rates from successive observations of nonmethane hydrocarbons in single air masses, *J. Geophys. Res.*, *112*, D10S40, doi:10.1029/2006JD007594.

Arnold, S. R., et al. (2015), Biomass burning influence on high-latitude tropospheric ozone and reactive nitrogen in summer 2008: A multi-model analysis based on POLMIP simulations, *Atmos. Chem. Phys.*, *15*, 6047–6068, doi:10.5194/acp-15-6047-2015.

Atkinson, R., D. L. Baulch, R. A. Cox, J. N. Crowley, R. F. Hampson, R. G. Hynes, M. E. Jenkin, M. J. Rossi, and J. Troe (2004), Evaluated kinetic and photochemical data for atmospheric chemistry: Volume I - gas phase reactions of Ox, HOx, NOx and SOx species, *Atmos. Chem. Phys.*, *4*, 1461–1738, doi:10.5194/acp-4-1461-2004.

Brown-Steiner, B., and P. Hess (2011), Asian influence on surface ozone in the United States: A comparison of chemistry, seasonality, and transport mechanisms, *J. Geophys. Res.*, *116*, D17309, doi:10.1029/2011JD015846.

Burkholder, J. B., S. P. Sander, J. Abbatt, J. R. Barker, R. E. Huie, C. E. Kolb, M. J. Kurylo, V. L. Orkin, D. M. Wilmouth, and P. H. Wine (2015), Chemical kinetics and photochemical data for use in atmospheric studies, Evaluation No. 18, JPL Publication 15-10, Jet Propul. Lab., Pasadena, Calif. [Available at http://jpldataeval.jpl.nasa.gov.]

Cain, M., J. Methven, and E. J. Highwood (2012), Quantification of chemical and physical processes influencing ozone during long-range transport using a trajectory ensemble, *Atmos. Chem. Phys.*, *12*, 7015–7039, doi:10.5194/acp-12-7015-2012.

Carl, S. (2005), A highly sensitive method for time-resolved detection of $O(^1D)$ applied to precise determination of absolute $O(^1D)$ reaction rate constants and $O(^3P)$ yields, *Phys. Chem. Chem. Phys.*, *7*(24), 4051–4053, doi:10.1039/B513576C.

Cooper, O. R., et al. (2010), Increasing springtime ozone mixing ratios in the free troposphere over Western North America, *Nature*, *463*, 344–348, doi:10.1038/nature08708.

Crowley, J. N., M. Ammann, R. A. Cox, R. G. Hynes, M. E. Jenkin, A. Mellouki, M. J. Rossi, J. Troe, and T. J. Wallington (2010), Evaluated kinetic and photochemical data for atmospheric chemistry: Volume V – heterogeneous reactions on solid substrates, *Atmos. Chem. Phys.*, *10*, 9059-9223, doi:10.5194/acp-10-9059-2010.

Evans, M. J., et al. (2000), Evaluation of a Lagrangian box model using field measurements from EASE (Eastern Atlantic Summer Experiment) 1996, *Atmos. Environ.*, *34*, 3843–3863.

Fehsenfeld, F. C., et al. (2006), International Consortium for Atmospheric Research on Transport and Transformation (ICARTT): North America to Europe—Overview of the 2004 summer field study, *J. Geophys. Res.*, *111*, D23S01, doi:10.1029/2006JD007829.

Folkins, I., R. Chatfield, D. Baumgardner, and M. Proffitt (1997), Biomass burning and deep convection in southeastern Asia: Results from ASHOE/MAESA, *J. Geophys. Res.*, *102*, 13,291–13,299, doi:10.1029/96JD03711.

Hollaway, M. J., S. R. Arnold, A. J. Challinor, and L. D. Emberson (2012), Intercontinental trans-boundary contributions to ozone- induced crop yield losses in the Northern Hemisphere, *Biogeosciences*, *9*, 271–292, doi:10.5194/bg-9-271-2012.

Ito, K., S. F. De Leon, and M. Lippmann (2005), Associations between ozone and daily mortality—Analysis and meta-analysis, *Epidemiology*, *16*, 446–457, doi:10.1097/01.ede.0000165821.90114.7f.

Jacob, D. J., J. A. Logan, and P. P. Murti (1999), Effect of rising Asian emissions on surface ozone in the U.S, *Geophys. Res. Lett.*, *26*, 2175–2178, doi:10.1029/1999GL900450.

Jaffe, D. A., I. McKendry, T. Anderson, and H. U. Price (2003), Six episodes of trans-Pacific transport of air pollutants, *Atmos. Environ.*, *37*, 391–404.

Kroll, J. H., and J. H. Seinfeld (2008), Chemistry of secondary organic aerosol: Formation and evolution of low-volatility organics in the atmosphere, *Atmos. Environ.*, *42*, 3593–3624.

Lelieveld, J., W. Peters, F. J. Dentener, and M. C. Krol (2002), Stability of tropospheric hydroxyl chemistry, *J. Geophys. Res.*, *107*(D23), 4715, doi:10.1029/2002JD002272.

Levy, J. I., T. J. Carrothers, J. T. Tuomisto, J. K. Hammitt, and J. S. Evans (2001), Assessing the public health benefits of reduced ozone concentrations, *Environ. Health Perspect.*, *109*, 1215–1226, doi:10.1289/ehp.011091215.

Lin, C. Y. C., D. J. Jacob, and A. M. Fiore (2001), Trends in exceedances of the ozone air quality standard in the continental United States, 1980–1998, *Atmos. Environ.*, *35*, 3217–3228.

Logan, J. A., M. J. Prather, S. C. Wofsy, and M. B. McElroy (1981), Tropospheric chemistry: A global perspective, *J. Geophys. Res.*, *86*, 7210–7354, doi:10.1029/JC086iC08p07210.

Mckay, M. D., R. J. Beckman, and W. J. Conover (2000), A comparison of three methods for selecting values of input variables in the analysis of output from a computer code, *Technometrics*, *42*(1), 55–61, doi:10.1080/00401706.2000.10485979.

Methven, J., et al. (2006), Establishing Lagrangian connections between observations within air masses crossing the Atlantic during the International Consortium for Atmospheric Research on Transport and Transformation experiment, *J. Geophys. Res.*, *111*, D23S62, doi:10.1029/2006JD007540.

Methven, J., S. R. Arnold, F. M. O'Connor, H. Barjat, K. Dewey, J. Kent, and N. Brough, (2003), Estimating photochemically produced ozone throughout a domain using flight data and a Lagrangian model, *J. Geophys. Res.*, *108*(D9), 4271, doi:10.1029/2002JD002955.

Myhre, G., et al. (2013), Anthropogenic and natural radiative forcing, in *Climate Change 2013: The Physical Science Basis. Contribution of Working Group I to the Fifth Assessment Report of the Intergovernmental Panel on Climate Change*, pp. 674–675, edited by T. F. Stocker et al., Cambridge Univ. Press, Cambridge, U. K., and New York.

Parrish, D. D., D. B. Millet, and A. H. Goldstein (2009), Increasing ozone in marine boundary layer inflow at the west coasts of North America and Europe, *Atmos. Chem. Phys.*, *9*, 1303–1323.

Price, H. U., D. A. Jaffe, O. R. Cooper, and P. V. Doskey (2004), Photochemistry, ozone production, and dilution during long-range transport episodes from Eurasia to the northwest United States, *J. Geophys. Res.*, *109*, D23S13, doi:10.1029/2003JD004400.

Pugh, T. A. M., et al. (2012), A Lagrangian model of air-mass photochemistry and mixing using a trajectory ensemble: The Cambridge Tropospheric Trajectory model of Chemistry And Transport (CiTTyCAT) version 4.2, *Geosci. Model Dev.*, *5*, 193–221, doi:10.5194/gmd-5-193-2012.

Rap, A., N. A. D. Richards, P. M. Forster, S. A. Monks, S. R. Arnold, and M. P. Chipperfield (2015), Satellite constraint on the tropospheric ozone radiative effect, *Geophys. Res. Lett.*, *42*, 5074–5081, doi:10.1002/2015GL064037.

Real, E., et al. (2007), Processes influencing ozone levels in Alaskan forest fire plumes during long-range transport over the North Atlantic, *J. Geophys. Res.*, *112*, D10S41, doi:10.1029/2006JD007576.

Real, E., et al. (2008), Lagrangian analysis of low altitude anthropogenic plume processing across the North Atlantic, *Atmos. Chem. Phys.*, *8*(24), 7737–7754.

Singh, H. B., et al. (2000), Biomass burning influences on the composition of the remote South Pacific troposphere: Analysis based on observations from PEM-Tropics-A, *Atmos. Environ.*, *34*, 635–644.

Sitch, S., P. M. Cox, W. J. Collins, and C. Huntingford (2007), Indirect radiative forcing of climate change through ozone effects on the land carbon sink, *Nature*, *448*(7155), 791–794, doi:10.1038/Nature06059.

Soldberg, S. and A. Lindskog (2005), The development of European surface ozone. Implications for a Revised Abatement Policy, EMEP/CCC-Report 1.

Stohl, A., C. Forster, S. Eckhardt, N. Spichtinger, H. Huntrieser, J. Heland, H. Schlager, S. Wilhelm, F. Arnold, and O. Cooper (2003), A backward modeling study of intercontinental pollution transport using aircraft measurements, *J. Geophys. Res.*, *108*(D12), 4370, doi:10.1029/2002JD002862.

Sudo, K., and H. Akimoto (2007), Global source attribution of tropospheric ozone: Long-range transport from various source regions, *J. Geophys. Res.*, *112*, D12302, doi:10.1029/2006JD007992.

Van Dingenen, R., F. J. Dentener, F. Raes, M. C. Krol, L. Emberson, and J. Cofala (2009), The global impact of ozone on agricultural crop yields under current and future air quality legislation, *Atmos. Environ.*, *43*, 604–618, doi:10.1016/j.atmosenv.2008.10.033.

Verstraeten, W. W., J. L. Neu, J. E. Williams, K. W. Bowman, J. R. Worden, and K. F. Boersma (2015), Rapid increases in tropospheric ozone production and export from China, *Nat. Geosci.*, *8*, 690–695, doi:10.1038/ngeo2493.

Young, P. J., et al. (2013), Pre-industrial to end 21st century projections of tropospheric ozone from the Atmospheric Chemistry and Climate Model Intercomparison Project (ACCMIP), *Atmos. Chem. Phys.*, *13*, 2063–2090, doi:10.5194/acp-13-2063-2013.

Zhang, Q., et al. (2009), Asian emissions in 2006 for the NASA INTEX-B mission, *Atmos. Chem. Phys.*, *9*, 5131–5153, doi:10.5194/acp-9-5131-2009.

Erratum

In the originally published version of this article, equation (1) incorrectly included the exponent $-\frac{\Delta E}{R}T$ instead of $-\frac{\Delta E}{RT}$. The equation has been amended, and the present version may be considered the authoritative version of record.